

Article

The Effects of Various Metallic Surfaces on Cellular and Bacterial Adhesion

Masaya Shimabukuro ¹, Haruka Ito ², Yusuke Tsutsumi ^{3,4}, Kosuke Nozaki ¹, Peng Chen ³, Risa Yamada ¹, Maki Ashida ³, Akiko Nagai ⁵ and Takao Hanawa ^{3,*}

¹ Graduate School of Medical and Dental Sciences, Tokyo Medical and Dental University, 1-5-45 Yushima, Bunkyo-ku, Tokyo 113-8549, Japan; shimabukuro.met@tmd.ac.jp (M.S.); k.nozaki.fpro@tmd.ac.jp (K.N.); ame.yamarisa666@gmail.com (R.Y.)

² Faculty of Dentistry, Tokyo Medical and Dental University, 1-5-45 Yushima, Bunkyo-ku, Tokyo 113-8549, Japan; 160072ds@tmd.ac.jp

³ Institute of Biomaterials and Bioengineering, Tokyo Medical and Dental University, 2-3-10 Kanda-Surugadai, Chiyoda-ku, Tokyo 101-0062, Japan; TSUTSUMI.Yusuke@nims.go.jp (Y.T.); chen.met@tmd.ac.jp (P.C.); ashida.met@tmd.ac.jp (M.A.)

⁴ Research Center for Structural Materials, National Institute for Materials Science (NIMS), 1-2-1 Sengen, Tsukuba, Ibaraki 305-0047, Japan

⁵ Department of Anatomy, School of Dentistry, Aichi Gakuin University, 1-100 Kusumoto, Chikusa-ku, Nagoya 464-8650, Japan; aknagai@dpc.agu.ac.jp

* Correspondence: hanawa.met@tmd.ac.jp; Tel.: +81-3-5280-8006; Fax: +81-3-5280-8006

Received: 22 September 2019; Accepted: 23 October 2019; Published: 25 October 2019



Abstract: The effects of Ti, Nb, Ta, Zr, and Ag on cellular and bacterial adhesion were investigated in this study. Moreover, the relationships between surface compositions, metal ion release behaviors, and biological responses were examined. As a result, MC3T3-E1 cells and *S. aureus* were able to better attach to Ti and Zr rather than the Nb and Ta specimens. For the Ag specimen, the amount of Ag ions released into Hanks' solution was the largest among all the specimens. Cellular and bacterial adhesion onto the Ag specimen was inhibited compared with the other specimens, because of Ag ion release. Alternatively, Nb and Ta specimens exhibited specific biological responses. Cellular adhesion on Nb and Ta specimens was similar to that on Ti, while bacterial adhesion on Nb and Ta specimens was inhibited compared with that on Ti. This study proved that Nb and Ta inhibited bacterial adhesion and exhibited no harmful effects on cellular adhesion. In addition, these results indicate that the passive layer on Nb and Ta plays a key role in the inhibition of bacterial adhesion.

Keywords: titanium; niobium; tantalum; zirconium; silver; β -stabilizer elements; antibacterial activity; biocompatibility; cytotoxicity; biofilm

1. Introduction

Titanium (Ti) and its alloys are widely used for medical and dental implant devices because of their high corrosion resistance, specific strength, and tissue compatibility. In addition, the interface reaction between Ti and bone tissue promotes bone formation and bone binding ability, a well-known advantage of the use of Ti for implant materials compared with other metals [1]. For artificial joints, bone fixators, spinal fixators, etc., the Young's modulus of the metal is greater than that of the cortical bone, so the load is not transmitted to the bone and stress shielding and finally, bone resorption may occur [2]. Therefore, implant devices must be constructed of materials with low Young's moduli that are close to that of cortical bone. Since the 1990s, β -type Ti alloys with low Young's moduli for the prevention of stress shielding in bone plates and stems of artificial hip joints in orthopedics have been developed [3–9]. β -type Ti alloys are comprised of Ti with

the β -stabilizer elements: niobium (Nb), tantalum (Ta), and zirconium (Zr). They are generally employed based on cell viability and the maintenance of a balance between corrosion resistance and biocompatibility in living tissue [9–15]. Nevertheless, little attention has been given to the antibacterial activities of Nb, Ta, and Zr. Recent studies have reported that biomaterial-associated infections caused by the formation of biofilms on biomaterial surfaces were a major cause of the failure of implant surgeries [16–19]. The biofilms are generally formed as a result of bacterial adhesion, growth, colony formation, extracellular polysaccharides, quorum sensing signals, and the formation of nutrition channels. Biofilms can weaken the effect of antibiotic agents because of the presence of a wide variety of bacterial species and the barrier effect of the extracellular polysaccharides [20–24]. After the formation of biofilms, it becomes almost impossible to remove the matured biofilms from implanted devices in the human body. The only way of preventing sepsis is by retrieving the device on which the biofilm was formed from the patient. To avoid this, antibacterial activity is necessary to inhibit biofilm formation during the implantation of devices. Silver (Ag) is a well-known antibacterial agent, and its effects on various bacteria have been studied extensively. Many researchers have reported that Ag can strongly influence various kinds of fungal and bacterial strains, including multidrug-resistant bacteria [25–28].

Therefore, we investigated the biological responses of alloying elements to β -type Ti alloys, Ti, Nb, Ta, and Zr, compared with Ag. The purpose of this study was to evaluate the adhesion of bacteria and osteogenic cells on Ti, Nb, Ta, Zr, and Ag. In addition, surface compositions and metal ion release behaviors were investigated by surface characterization and dissolution testing, respectively. Biological responses were investigated by *in vitro* tests using *Staphylococcus aureus* (*S. aureus*) and MC3T3-E1 osteogenic cells.

2. Materials and Methods

2.1. Specimen Preparation

Commercially pure Ti (Grade 2), Nb ($\geq 99.98\%$), Ta ($\geq 99.98\%$), Zr ($\geq 99.2\%$), and Ag (99.99%) rods were employed in this study. Each metal disk was prepared by mechanical cutting. The surfaces of the disks were mechanically polished using #150, #320, #600, and #800 grid SiC abrasive papers, followed by ultra-sonication in acetone and ethanol for 10 min. After ultra-sonication, the specimens were immersed in ultrapure water at ambient temperature (25 °C) for 24 h to stabilize the passive layer. The disks were then stored in an auto-dry desiccator until further use.

2.2. XPS Measurement

X-ray photoelectron spectroscopy (XPS) was performed using a spectrometer (JPS-9010MC, JEOL, Tokyo, Japan) with a Mg K α X-ray source (energy: 1253.6 eV; acceleration voltage: 10 kV; current: 10 mA). The pressure of the measurement chamber was 1×10^{-7} Pa. All binding energies mentioned in this study are relative to the Fermi level. The spectrometer was calibrated against Au 4f $_{7/2}$ of pure gold, Ag 3d $_{5/2}$ of pure silver, and Cu 2p $_{3/2}$ of pure copper. The detection angle to the specimen surface was 90°. The binding energies were calibrated with the C 1s electron energy region peak derived from contaminating carbon (285.0 eV). To calculate the integrated intensity of peaks, the background was subtracted from the measured spectrum according to Shirley's method [29]. The composition of the specimens was calculated according to a method described previously [30]. The photoionization cross-section of empirical data [31,32] and theoretically calculated data [33] was used for quantification.

2.3. Dissolution Test

The dissolution test was performed to evaluate the amount of metal ions released from the specimens during the immersion in Hanks' solution. The composition of Hanks' solution was 1.37×10^{-1} mol L $^{-1}$ NaCl, 5.37×10^{-3} mol L $^{-1}$ KCl, 1.26×10^{-3} mol L $^{-1}$ CaCl $_2$, 4.23×10^{-4} mol L $^{-1}$

Na_2HPO_4 , $4.41 \times 10^{-4} \text{ mol L}^{-1}$ KH_2PO_4 , $7.39 \times 10^{-4} \text{ mol L}^{-1}$ Mg_2SO_4 , and $4.17 \times 10^{-3} \text{ mol L}^{-1}$ NaHCO_3 . The specimens were immersed in the test solution (5 mL) at 310 K for 24 h. The pH value of the test solution was confirmed to be within the range of 7.40 ± 0.05 and was prepared immediately before use. Hanks' solution without organic species with ion concentrations similar to those of extracellular fluid was employed as the test solution [34]. After 72 h immersion, the concentrations of the metal ions were evaluated using inductively coupled plasma-atomic emission spectrometry (ICP-AES, ICPS-7000 ver. 2, Shimadzu Corp., Kyoto, Japan).

2.4. Cellular Adhesion Test

As described in our previous work [35], MC3T3-E1 cells (RIKEN BioResource Center, Tsukuba, Japan) were maintained in cell culture medium: alpha modification of Eagle's minimum essential medium (α -MEM; GIBCO, Grand island, CA, USA) supplemented with 10% fetal bovine serum (FBS; GIBCO), 10 U mL^{-1} penicillin, 100 mg mL^{-1} streptomycin, and 0.25 mg mL^{-1} amphotericin B (GIBCO). All specimens were sterilized in 70% ethanol for 20 min and thoroughly rinsed with deionized water before *in vitro* testing. The cells were seeded on to the sterilized specimens with an approximate initial density of $10,000 \text{ cells cm}^{-2}$. The cells were incubated at 37°C in a fully humidified atmosphere under 5% CO_2 .

After the seeding for 24 h, the cells attached to each specimen were harvested with trypsin/EDTA, re-suspended in a cell culture medium, and transferred to 96-well microplates. Then, the Cell Counting Kit-8 assay (CCK-8, Dojindo Laboratories, Kumamoto, Japan) was added to each 96-well microplate, which contained cell suspension, and the reaction was continued for 4 h at 37°C . The absorbance of the samples was measured at 450 nm using a microplate reader (ChroMate Microplate Reader, Awareness Technology, Palm City, FL, USA). The reference wavelength was set at 630 nm. In this evaluation, the tissue culture polystyrene (TCPS) was used as a control specimen for the quantification of the number of attached cells on each specimen. The cells attached on the TCPS were harvested by treatment with Trypsin/EDTA, followed by the re-suspension of cells in the cell culture medium. Cell suspensions were diluted serially. The number of cells in cell suspension harvested from TCPS were counted by trypan blue (Trypan Blue Stain 0.4%; Gibco) using a hemocytometer. Then, standard curves for cell number calibration and for light absorbance were constructed and used for the quantification of the number of attached cells on each specimen.

2.5. Bacteria Adhesion Test

The antibacterial activity was evaluated according to the ISO 22196: 2007 method. To examine the antibacterial activity of the specimens, we employed *S. aureus* (NBRC122135). The experiment was approved by the Pathogenic Organisms Safety Management Committee in Tokyo Medical and Dental University (22012-025c). *S. aureus* is Gram-positive cocci frequently found in the nose, respiratory tract, and on the skin. *S. aureus* was cultured in tryptic soy broth (TryptoSoya Broth, Nissui, Tokyo, Japan) at 37°C for 24 h. The optical density of the bacterial suspensions was measured at 600 nm using an ultraviolet-visible (UV-vis) spectrometer (V-550, JASCO, Tokyo, Japan) and diluted to obtain concentrations of $5.5\text{--}10 \times 10^5$ colony-forming units (CFUs) mL^{-1} . Prior to the antibacterial activity testing, all specimens were sterilized with 70% ethanol, washed with distilled water, and dried. Drops of bacterial suspension were added onto all specimens, which were subsequently covered with a sterilized plastic film and incubated at 37°C for 24 h ($n = 3$). Bacterial cells were then collected from all the incubated specimens; the obtained suspensions were diluted, pipetted onto nutrient agar plates, and incubated overnight at 37°C . The number of viable bacteria was determined by counting the number of colonies formed. In addition, (\pm)-6-Hydroxy-2,5,7,8-tetramethylchromane-2-carboxylic acid (Trolox, Sigma-Aldrich, Tokyo, Japan) was used as a scavenger to investigate the effects of reactive oxygen species for bacteria. Drops of bacterial suspension with 0.05 mM Trolox were added onto the Nb and Ta specimens, which were subsequently covered with a sterilized plastic film and incubated at 37°C for 24 h ($n = 3$). Bacterial cells were then collected from all the incubated specimens; the

obtained suspensions were diluted, pipetted onto nutrient agar plates, and incubated overnight at 37 °C. The number of viable bacteria was determined by counting the number of colonies formed.

2.6. Statistical Analysis

Data were calculated from five independent specimens. All values are presented as means \pm SD, and commercial statistical software KaleidaGraph (Synergy Software, Reading, PA, USA) was used for statistical analysis. One-way analysis of variance was used following multiple comparisons with the Student–Newman–Keuls method to assess the data, and $p < 0.05$ was considered to indicate statistical significance.

3. Results

3.1. XPS Measurement

Figure 1 shows the XPS survey scan spectra obtained from each specimen. The peaks originating from C 1s and O 1s orbital binding energies were detected from the spectra obtained from all specimens. Moreover, each peak originated from the Ti 2p, Nb 3d, Ta 4f, Zr 3d, and Ag 3d binding energies were detected from each metallic specimen, respectively. The XPS spectra of Ti 2p, Nb 3d, Ta 4f, Zr 3d, Ag 3d, and the O 1s electron binding energy regions obtained from the specimens are shown in Figure 2. The deconvolution of peaks was conducted according to the published data with compatible full-width of half-maximum values [36–40]. As a result, the spectra of Ti, Nb, Ta, and Zr were identified as metallic (Ti^0 , Nb^0 , Ta^0 , and Zr^0) and oxidized states (Ti^{2+} , Ti^{3+} , Ti^{4+} , Nb^{2+} , Nb^{4+} , Nb^{5+} , Ta^{5+} , and Zr^{4+}). Moreover, the spectra of O 1s obtained from Ti, Nb, Ta, and Zr specimens were composed of three peaks, originating from O^{2-} , OH^- , and H_2O . Alternately, the spectrum of Ag was identified as only the metallic state (Ag^0). The spectrum of O 1s obtained from the Ag specimen showed a low-intensity peak and was composed of OH^- and H_2O .

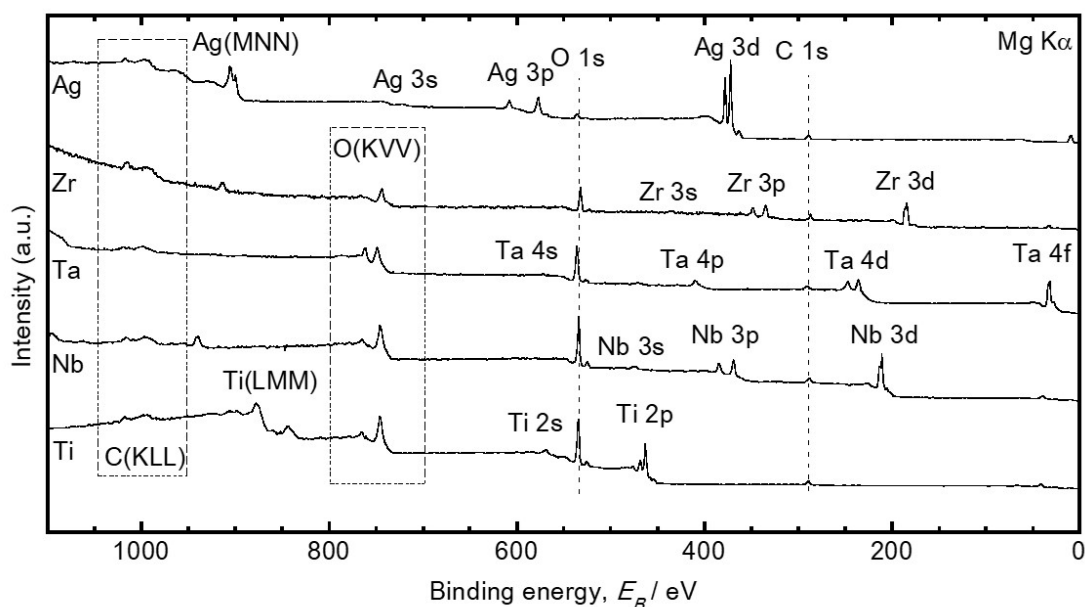


Figure 1. X-ray photoelectron spectroscopy survey (XPS) spectra obtained from the Ti, Nb, Ta, Zr, and Ag specimens. The spectra obtained from Ti, Nb, Ta, Zr, and Ag are arranged from the bottom, respectively.

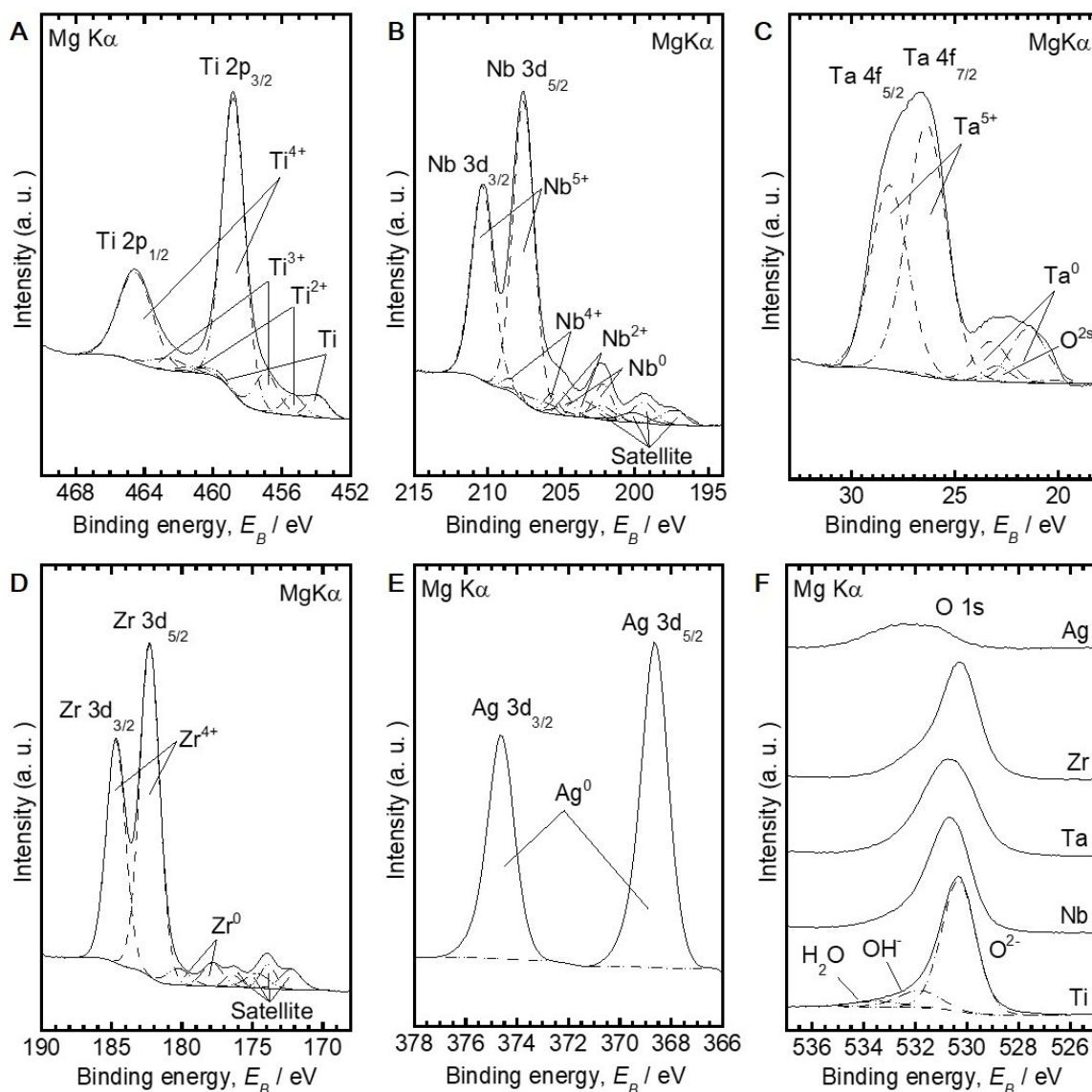


Figure 2. XPS narrow scan spectra around (A) Ti 2p, (B) Nb 3d, (C) Ta 4f, (D) Zr 3d, (E) Ag 3 d, and (F) O 1s electron binding energy regions obtained from the specimens.

The composition and thickness of the passive layer on each metal specimen calculated from the XPS measurement with a detection angle of 90° are summarized in Table 1. The compositions of the passive layer on Ti, Nb, Ta, and Zr specimens consisted almost entirely of 70 at.% oxygen and 30 at.% metal. Moreover, the thickness of the passive layer was 5.5 to 6.2 nm. However, the surface composition of Ag was different from those of the other specimens. The thickness of the surface oxide layer could not be calculated because of the slight peak of O 1s and the Ag 3d peak composed only of Ag^0 .

Table 1. The composition and thickness of the passive layer on each metal specimen calculated from the XPS measurement with a detection angle of 90°.

Specimen	Composition (at.%)						Thickness (nm)
	O	Ti	Nb	Ta	Zr	Ag	
Ti	71	29	-	-	-	-	6.1
Nb	70	-	30	-	-	-	6.2
Ta	71	-	-	29	-	-	5.5
Zr	66	-	-	-	34	-	5.9
Ag	26	-	-	-	-	74	-

3.2. Dissolution Test

Figure 3 shows the amount of metal ions released from the specimens during 72 h immersion in Hanks' solution. Ti, Nb, Zr and Ag ions were released from the specimens immersed in Hanks' solution. Ta ions were not detected in this test condition. The amount of each metal ion released per unit area and converted to the molar concentration was $3.1 \times 10^{-8} \text{ mol L}^{-1}$ (Ti ions), $8.6 \times 10^{-9} \text{ mol L}^{-1}$ (Nb ions), $1.1 \times 10^{-6} \text{ mol L}^{-1}$ (Zr ions), and $1.9 \times 10^{-6} \text{ mol L}^{-1}$ (Ag ions). Therefore, Ag ions were the most eluted in this test condition.

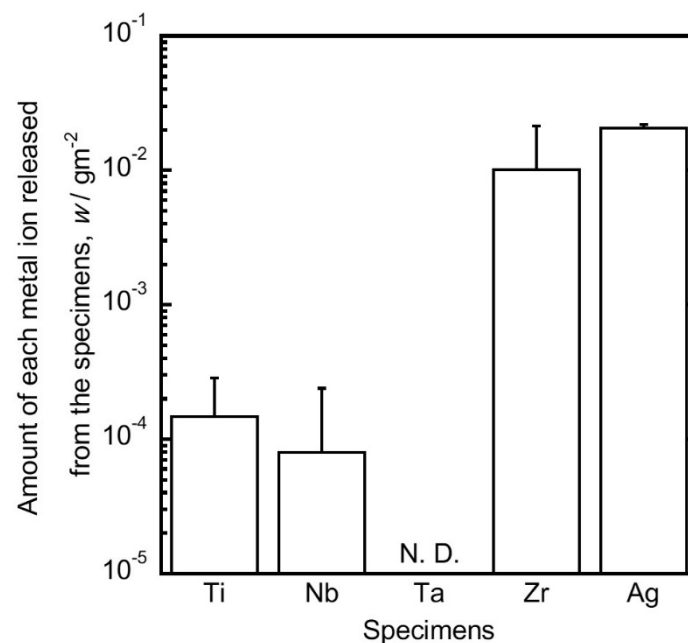


Figure 3. The amount of metal ions released from specimens during 72 h immersion in Hanks' solution. Data are shown as the mean \pm SD. N. D.: not detected.

3.3. Cellular Adhesion Test

The results of cellular adhesion testing using MC3T3-E1 cells after seeding for 24 h are shown in Figure 4. There were no significant differences between the numbers of viable cells attached to Ti, Nb, Ta, and Zr specimens. However, the number of viable cells attached to Ag specimens was significantly lower than those on the other specimens.

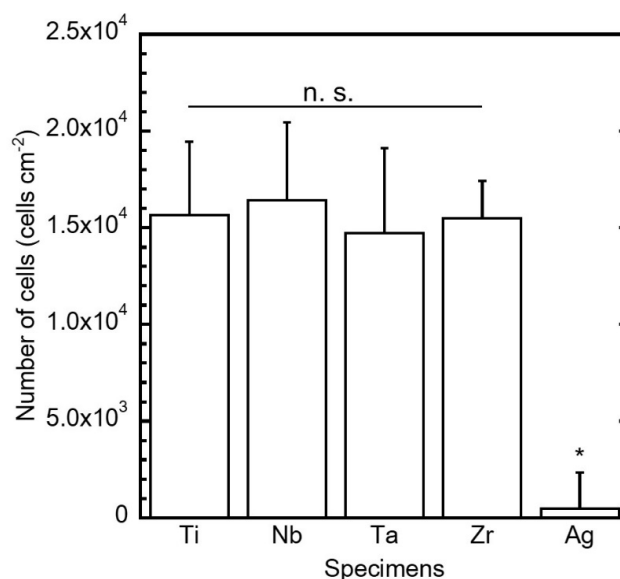


Figure 4. The number of living cells on each specimen 24 h after seeding. Data are shown as the mean \pm SD. *: Significant difference; n.s.: No significant difference (ANOVA + Student-newman-keuls (SNK) ($p < 0.05$, $N = 5$)).

3.4. Bacteria Adhesion Test

Figure 5 shows the normalized CFU count for *S. aureus*, demonstrating the antibacterial effects of the specimens. The vertical axis represents the normalized bacterial number, defined as the bacterial number on each of the specimens divided by the initial number of *S. aureus*. A normalized bacterial number that was below 1 (shown as a dashed line in the figure) implied that the tested specimen had antibacterial activity. There were no significant differences between the *S. aureus* counts on the Ti and Zr specimens. However, antibacterial effects of the Nb, Ta, and Ag specimens were observed; the *S. aureus* counts on these specimens were significantly lower than those on the Ti specimen. In particular, the Ag specimen was most effective against *S. aureus*. The Nb and Ta specimens exhibited a sufficient effect compared to the Ti specimen and could inhibit the adhesion of *S. aureus*.

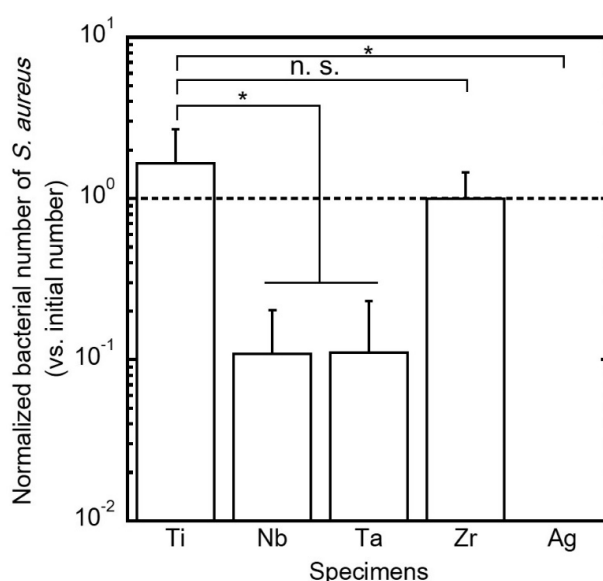


Figure 5. The number of *S. aureus* attached to each specimen 24 h after seeding. Data are shown as the mean \pm SD. *: Significant difference against Ti; n.s.: No significant difference against Ti (ANOVA + SNK) ($p < 0.05$, $N = 5$)).

Figure 6 shows the normalized CFU count for *S. aureus*, demonstrating the antibacterial effects of the specimens in the suspension with and without Trolox. The vertical axis represents the normalized bacterial number, defined as the bacterial number on each of the specimens divided by the number of *S. aureus* in the suspension without Trolox on each specimen. A normalized bacterial number that was above 1 (shown as dashed line in the figure) implied that the antibacterial activity of the tested specimen was reduced by the Trolox. The *S. aureus* counts in the suspension with Trolox on Nb and Ta were significantly higher than those without Trolox. Therefore, the antibacterial effects of Nb and Ta were reduced by Trolox.

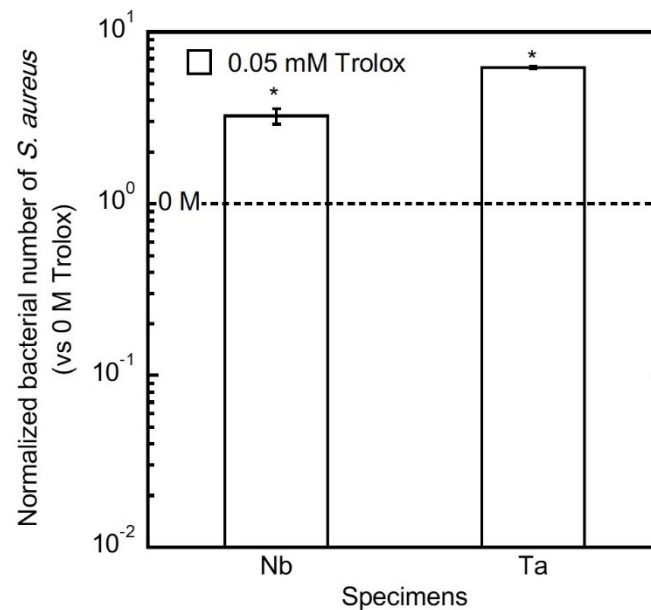


Figure 6. The number of *S. aureus* in 0 and 0.05 mM Trolox-containing bacterial suspension incubated on each specimen. Data are shown as the mean \pm SD. *: Significant difference against 0 M Trolox. (ANOVA + SNK ($p < 0.05$, $N = 5$)).

4. Discussion

The passive layers composed of approximately 70 at.% oxygen and 30 at.% metallic elements were confirmed for the Ti, Nb, Ta, and Zr specimens. The passive layers on these specimens were of almost the same thickness (Figures 1 and 2, Table 1). Generally, valve metals such as Ti, Nb, Ta, and Zr have good corrosion resistance. However, a small amount of Ti, and Nb ions were released from the specimen in this test condition. Although a relatively large amount of Zr ions was eluted, Ta was not eluted (Figure 3). These metal specimens may release a small amount of their ions in some situations in vivo. Nevertheless, MC3T3-E1 cells were able to attach to Ti, Nb, Ta, and Zr specimens (Figure 4). This indicates that their surface compositions and metal ion release behaviors did not affect the adhesion of MC3T3-E1 cells. This demonstrates that these metals are suitable Ti alloying elements for in vivo use. Yamamoto et al. reported that the IC_{50} s of Ti, Nb, Ta, and Zr ions for MC3T3-E1 cells was $8.7 \times 10^{-4} \text{ mol L}^{-1}$ (Ti ions), $1.5 \times 10^{-3} \text{ mol L}^{-1}$ (Nb ions), $2.1 \times 10^{-3} \text{ mol L}^{-1}$ (Ta ions), and $2.8 \times 10^{-3} \text{ mol L}^{-1}$ (Zr ions) [41]. Therefore, it is possible that MC3T3-E1 cells were able to attach to each metal because the amount of each metal ion released into Hanks' solution during the 72 h period did not reach the IC_{50} s for MC3T3-E1 cells. In other words, Ti, Nb, Ta, and Zr had no harmful effects on the cellular viability of the osteogenic cells and may exhibit good osteogenic cell compatibility, at least during the initial phase of implantation. Moreover, focusing on the biological properties of Nb and Ta, Matsuno et al. implanted Nb and Ta wires into the subcutaneous tissue of the abdominal region and into the femoral bone marrow of rats for either 2 or 4 weeks. They concluded that Nb and Ta

had good biocompatibility and osteoconductivity, based on confirmation of new bone formation [42]. These results provide adequate evidence that Nb and Ta had good osteogenic cell compatibility.

Metals that are not valve metals usually do not passivate, and similar results were obtained from the Ag specimen in this study (Figures 1 and 2, Table 1). The amount of Ag ions released from the specimen into the Hanks' solution was 1.9×10^{-6} mol L⁻¹ (Figure 3). Yamamoto et al. reported that the IC₅₀ of Ag ions for MC3T3-E1 cells was 2.8×10^{-6} mol L⁻¹ [41]. Therefore, the amount of Ag ions released into the test solution during 72 h almost reached the IC₅₀ for MC3T3-E1 cells. Moreover, the adhesion of MC3T3-E1 cells was inhibited on the Ag specimen compared with the other specimens (Figure 4). These phenomena indicate that the surface composition of the Ag specimen and the Ag ion release behavior have a high potential to be cytotoxic and may affect bone tissue.

Bacterial adhesion of *S. aureus* was inhibited on the Nb, Ta, and Ag specimens compared with that on the Ti specimen (Figure 5). In the case of the Ag specimen, the amount of Ag ions released from the specimen was the largest among all specimens. The IC₅₀ of Ag ions for MC3T3-E1 cells was the lowest compared with those of Ti, Nb, Ta, and Zr ions [41]. Therefore, it is possible that the Ag antibacterial effect against *S. aureus* was due to Ag ion release. However, the amount of Nb and Ta ions released from each specimen was lower than that of the Ag ion. In general, it is known that the effectiveness of Ag ions against cells is higher than that of Nb and Ta ions [41]. Therefore, Nb and Ta ions released from the specimens did not affect the bacterial adhesion of *S. aureus*. The results of surface characterization by XPS showed that passive layers were confirmed on the Nb and Ta specimens. Each film was composed of an oxide state (Nb²⁺, Nb⁴⁺, Nb⁵⁺, and Ta⁵⁺) and a metallic state (Nb⁰ and Ta⁰) (Figures 1 and 2, Table 1). Based on these results, it is possible that each metal oxide, as a passive layer, plays a key role in the development of antibacterial effects against bacterial adhesion. Ziolk et al. reported that reactive oxygen specimens (ROS) intermediates were generated on the surface of amorphous Nb₂O₅ and Ta₂O₅ upon interaction with aqueous H₂O₂ [43]. This study revealed that the antibacterial effects of Nb and Ta were reduced by Trolox (Figure 6). Since Trolox usually acts as the scavenger of ROS, it is considered that the antibacterial effects of Nb and Ta were reduced by the antioxidant action of Trolox. Therefore, we believe that the antibacterial effects of Nb and Ta specimens were due to the generation of ROS on their surface. Regarding the valences of Nb and Ta in the passive layer, Nb and Ta exist in a maximum pentavalent oxidation state. For this reason, Nb and Ta oxides tend to exhibit the characteristics of an n-type semiconductor. Hence, the antibacterial effects of Nb and Ta are the result of their passive layers. However, a more detailed examination related to the generation of ROS on the Nb and Ta surface is necessary in the future. The balances between cellular viability and the bacterial adhesion on Nb and Ta were superior compared with those on the other specimens. Therefore, Nb and Ta are useful not only as β-stabilizers but also as antibacterial elements without any cytotoxicity. On the other hand, Ag exhibited antibacterial activity with cytotoxicity. Therefore, controlling the concentration of Ag is necessary for its use on the implant surface. Some researchers have reported that Ti–Ag alloys show good corrosion resistance and improved mechanical properties compared to Ti [44,45]. In addition, Kang et al. reported that surface-treated Ti–Ag alloys exhibited antibacterial activity without cytotoxicity [46]. Therefore, suitable amounts of Ag are useful not only as antibacterial elements but also as additive elements for implant materials.

We hope that in the future, the outcome of the present study will be useful in the design of biocompatible implant materials.

5. Conclusions

The biological responses, surface compositions, and metal ion release behaviors of Ti, Nb, Ta, Zr, and Ag specimens were investigated in this study. MC3T3-E1 cells and *S. aureus* were able to better adhere to the Ti and Zr specimens than the Nb and Ta specimens. The Ag specimen inhibited both cellular viability and bacterial adhesion, owing to Ag ion release. Alternatively, Nb and Ta specimens inhibited only bacterial adhesion and exhibited no harmful effects on cellular viability. Therefore, Nb and Ta are useful as non-cytotoxic antibacterial elements.

Author Contributions: M.S., Y.T., A.N., and T.H. conceived and designed the experiments. M.S., H.I., M.A., P.C., R.Y. and K.N. performed the experiments; and M.S., P.C., and K.N. analyzed the data. M.S. and T.H. contributed to material preparation; M.S. and T.H. wrote the paper.

Funding: This research received no external funding.

Acknowledgments: This study was supported by the Research Center for Biomedical Engineering, Tokyo Medical and Dental University, Project “Creation of Life Innovation Materials for Interdisciplinary and International Researcher Development” and project “Cooperative project amount medicine, dentistry, and engineering for medical innovation-Construction of creative scientific research of the viable material via integration of biology and engineering” by the Ministry of Education, Culture, Sports, Science and Engineering, Japan.

Conflicts of Interest: The authors declare no conflict of interest.

References

1. Hanawa, T. Titanium—Tissue interface reaction and its control with surface treatment. *Front. Bioeng. Biotechnol.* **2019**, *17*, 170. [[CrossRef](#)] [[PubMed](#)]
2. Gefen, A. Computational simulations of stress shielding and bone resorption around existing and computer-designed orthopaedic screws. *Med. Biol. Eng. Comput.* **2002**, *40*, 311–322. [[CrossRef](#)] [[PubMed](#)]
3. Wang, K.; Gustavson, L.; Dumbleton, J. Low modulus, high strength, biocompatible titanium alloy for medical implants. In *Titanium'92*; Froes, F.H., Caplan, H.L., Eds.; TMS: Warrenda, PA, USA, 1992; pp. 2697–2704.
4. Zardiackas, L.D.; Mitchell, D.W.; Disegi, J.A. Characterization of Ti-15Mo beta titanium alloy for orthopaedic implant applications. In *Medical Applications of Titanium and Its Alloys*; Browns, S.A., Lemons, J.E., Eds.; ASTM: West Conshohoken, PA, USA, 1996; pp. 60–75.
5. Fanning, J.C. Properties and processing of a new metastable beta titanium alloy for surgical implant applications. In *Titanium'95*; Blenkinsop, P.A., Evans, W.J., Flower, H., Eds.; The University Press: Cambridge, UK, 1996; pp. 1800–1807.
6. Rao, V.B.; Houska, C.R. Kinetics of the phase-transformation in a Ti-15Mo-5Zr-3Al alloy as studied by X-ray-diffraction. *Metall. Trans. A* **1979**, *10*, 355–358. [[CrossRef](#)]
7. Matsuda, Y.; Nakamura, T.; Ido, K.; Oka, M.; Okumura, H.; Matsushita, T. Femoral component made of Ti-15Mo-5Zr-3Al alloy in total hip arthroplasty. *J. Orthop. Sci.* **1997**, *2*, 166–170. [[CrossRef](#)]
8. Okazaki, Y. A New Ti-15Zr-4Nb-4Ta alloy for medical applications. *Curr. Opin. Solid State Mater. Sci.* **2001**, *5*, 45–53. [[CrossRef](#)]
9. Niinomi, M. Design and development of metallic biomaterials with biological and mechanical biocompatibility. *J. Biomed. Mater. Res. A* **2019**, *107*, 944–954. [[CrossRef](#)]
10. Geetha, M.; Singh, A.K.; Asokamani, R.; Gogia, A.K. Ti based biomaterials, the ultimate choice for orthopaedicimplants—A review. *Prog. Mater. Sci.* **2009**, *54*, 397–425. [[CrossRef](#)]
11. Niinomi, M.; Nakai, M.; Hieda, J. Development of new metallic alloys for biomedical applications. *Acta Biomater.* **2012**, *8*, 3888–3903. [[CrossRef](#)]
12. Wang, K. The use of titanium for medical applications in the USA. *Mater. Sci. Eng. A* **1996**, *213*, 134–137. [[CrossRef](#)]
13. Niinomi, M. Recent metallic materials for biomedical applications. *Metall. Mater. Trans. A Phys. Metall. Mater. Sci.* **2002**, *33*, 477–486. [[CrossRef](#)]
14. Okazaki, Y.; Ito, Y.; Kyo, K.; Tateishi, T. Corrosion resistance and corrosion fatigue strength of new titanium alloys for medical implants without V and Al. *Mater. Sci. Eng. A Struct. Mater.* **1996**, *213*, 138–147. [[CrossRef](#)]
15. Kawahara, H.; Yamagami, A.; Nakamura, M. Biological testing of dental materials by means of tissue culture. *Int. Dent. J.* **1968**, *18*, 443–467. [[PubMed](#)]
16. Dibart, S.; Warbington, M.; Su, M.F.; Skobe, Z. In vitro evaluation of the implant-abutment bacterial seal: The locking taper system. *Int. J. Oral Maxillofac. Implant.* **2005**, *20*, 732–737.
17. Glauser, R.; Schupbach, P.; Gottlow, J.; Hammerle, C.H.F. Periimplant soft tissue barrier at experimental one-piece mini-implants with different surface topography in humans: A light-microscopic overview and histometric analysis. *Clin. Implant Dent. Relat. Res.* **2005**, *7*, S44–S51. [[CrossRef](#)]
18. Tesmer, M.; Wallet, S.; Koutouzis, T.; Lundgren, T. Bacterial colonization of the dental implant fixture-abutment interface: An in vitro study. *J. Periodontol.* **2009**, *80*, 1991–1997. [[CrossRef](#)]

19. MacKintosh, E.E.; Patel, J.D.; Marchant, R.E.; Anderson, J.M. Effects of biomaterial surface chemistry on the adhesion and biofilm formation of *Staphylococcus epidermidis* in vitro. *J. Biomed. Mater. Res. A* **2006**, *78*, 836–842. [[CrossRef](#)]
20. Lindsay, D.; von Holy, A. Bacterial biofilms within the clinical setting: What healthcare professionals should know. *J. Hosp. Infect.* **2006**, *64*, 313–325. [[CrossRef](#)]
21. Fux, C.A.; Costerton, J.W.; Stewart, P.S.; Stoodley, P. Survival strategies of infectious biofilms. *Trends. Microbiol.* **2005**, *13*, 34–40. [[CrossRef](#)]
22. Stewart, P.S.; Costerton, J.W. Antibiotic resistance of bacteria in biofilms. *Lancet* **2001**, *358*, 135–138. [[CrossRef](#)]
23. Hoiby, N.; Bjarnsholt, T.; Givskov, M.; Molin, S.; Ciofu, O. Antibiotic resistance of bacterial biofilms. *Int. J. Antimicrob. Agents* **2010**, *34*, 322–332. [[CrossRef](#)]
24. Koo, H.; Allan, R.N.; Howlin, R.P.; Stoodley, P.; Hall-Stoodley, L. Targeting microbial biofilms: Current and prospective therapeutic strategies. *Nat. Rev. Microbiol.* **2017**, *15*, 740–755. [[CrossRef](#)] [[PubMed](#)]
25. Cochis, A.; Azzimonti, B.; Della Valle, C.; De Giglio, E.; Bloise, N.; Visai, L.; Cometa, S.; Rimondini, L.; Chiesa, R. The effect of silver or gallium doped titanium against the multidrug resistant *Acinetobacter baumannii*. *Biomaterials* **2016**, *80*, 80–95. [[CrossRef](#)] [[PubMed](#)]
26. Rai, M.K.; Deshmukh, S.D.; Ingle, A.P.; Gade, A.K. Silver nanoparticles: The powerful nanoweapon against multidrug-resistant bacteria. *J. Appl. Microbiol.* **2012**, *112*, 841–852. [[CrossRef](#)] [[PubMed](#)]
27. Lara, H.H.; Ayala-Nunez, N.V.; Turrent, L.D.I.; Padilla, C.R. Bactericidal effect of silver nanoparticles against multidrug-resistant bacteria. *World J. Microbiol. Biotechnol.* **2010**, *26*, 615–621. [[CrossRef](#)]
28. Prakash, P.; Gnanaprakasam, P.; Emmanuel, R.; Arokiyaraj, S.; Saravanan, M. Green synthesis of silver nanoparticles from leaf extract of *Mimusops elengi*, Linn. for enhanced antibacterial activity against multi drug resistant clinical isolates. *Colloids Surf. B Biointerfaces* **2013**, *108*, 255–259. [[CrossRef](#)] [[PubMed](#)]
29. Shirley, D.A. High-Resolution X-Ray Photoemission Spectrum of the Valence Bands of Gold. *Phys. Rev. B* **1972**, *5*, 552–556. [[CrossRef](#)]
30. Asami, K.; Hashimoto, K.; Shimodaira, S. XPS determination of compositions of alloy surfaces and surface oxides on mechanically polished iron–chromium alloys. *Corros. Sci.* **1977**, *17*, 713–723. [[CrossRef](#)]
31. Asami, K.; Chen, S.C.; Habazaki, H.; Kawashima, A.; Hashimoto, K. A photoelectrochemical and ESCA study of passivity of amorphous nickel–vanadium metal alloys. *Corros. Sci.* **1990**, *31*, 727–732. [[CrossRef](#)]
32. Hashimoto, K.; Kasaya, M.; Asami, K.; Masumoto, T. Electrochemical and XPS studies on corrosion behavior of amorphous Ni–Cr–P–B alloys. *Corros. Eng.* **1977**, *26*, 445–452. [[CrossRef](#)]
33. Scofield, J.H. Hartree-Slater subshell photoionization cross-sections at 1254 and 1487 eV. *J. Electron Spectrosc. Relat. Phenom.* **1976**, *8*, 129–137. [[CrossRef](#)]
34. Tsutsumi, Y.; Nishimura, D.; Doi, H.; Nomura, N.; Hanawa, T. Difference in surface reactions between titanium and zirconium in Hanks' solution to elucidate mechanism of calcium phosphate formation on titanium using XPS and cathodic polarization. *Mater. Sci. Eng. C Biomim. Supramol. Syst.* **2009**, *29*, 1702–1708. [[CrossRef](#)]
35. Oya, K.; Tanaka, Y.; Moriyama, Y.; Yoshioka, Y.; Kimura, T.; Tsutsumi, Y.; Doi, H.; Nomura, N.; Noda, K.; Kishida, A.; et al. Differences in the bone differentiation properties of MC3T3-E1 cells on polished bulk and sputter-deposited titanium specimens. *J. Biomed. Mater. Res. A* **2010**, *94*, 611–618. [[CrossRef](#)] [[PubMed](#)]
36. NIST X-ray Photoelectron Spectroscopy Database, Version 4.1 (National Institute of Standards and Technology, Gaithersburg, 2012). Available online: <http://srdata.nist.gov/xps/> (accessed on 18 July 2019).
37. Moulder, J.F.; Stickle, W.F.; Sobol, P.E.; Bomben, K.D. *Handbook of X-ray Photoelectron Spectroscopy*; Perkin-Elmer Corp: Eden Prairie, MN, USA, 1992.
38. Asami, K.; Chen, S.C.; Habazaki, H.; Hashimoto, K. The surface characterization of titanium and titanium–nickel alloys in sulfuric acid. *Corros. Sci.* **1993**, *35*, 43–49. [[CrossRef](#)]
39. Tsutsumi, Y.; Nishisaka, T.; Doi, H.; Ashida, M.; Chen, P.; Hanawa, T. Reaction of calcium and phosphate ions with titanium, zirconium, niobium, and tantalum. *Surf. Interface Anal.* **2015**, *47*, 1148–1154. [[CrossRef](#)]
40. Tanaka, Y.; Nakai, M.; Akahori, T.; Niinomi, M.; Tsutsumi, Y.; Doi, H.; Hanawa, T.; Matsuno, H. Characterization of air-formed surface oxide film on Ti–29Nb–13Ta–4.6Zr alloy surface using XPS and AES. *Corros. Sci.* **2008**, *50*, 2111–2116. [[CrossRef](#)]
41. Yamamoto, A.; Honma, R.; Sumita, M. Cytotoxicity evaluation of 43 metal salts using murine fibroblasts and osteoblastic cells. *J. Biomed. Mater. Res.* **1998**, *39*, 331–340. [[CrossRef](#)]

42. Yokoyama, A.; Watari, F.; Uo, M.; Kawasaki, T. Biocompatibility and osteogenesis of refractory metal implants, titanium, hafnium, niobium, tantalum and rhenium. *Biomaterials* **2001**, *22*, 1253–1262.
43. Ziolk, M.; Sobczak, I.; Decyk, P.; Sobanska, K.; Pietrzyk, P.; Sojka, Z. Search for reactive intermediates in catalytic oxidation with hydrogen peroxide over amorphous niobium(V) and tantalum(V) oxides. *Appl. Catal. B* **2015**, *164*, 288–296. [[CrossRef](#)]
44. Zhang, B.B.; Zheng, Y.F.; Liu, Y. Effect of Ag on the corrosion behavior of Ti–Ag alloys in artificial saliva solutions. *Dent. Mater.* **2009**, *25*, 672–677. [[CrossRef](#)]
45. Shim, H.M.; Oh, K.T.; Woo, J.Y.; Hwang, C.J.; Kim, K.N. Corrosion resistance of titanium–silver alloys in an artificial saliva containing fluoride ions. *J. Biomed. Mater. Res. B* **2005**, *73*, 252–259. [[CrossRef](#)]
46. Kang, M.K.; Moon, S.K.; Kwon, J.S.; Kim, K.M.; Kim, K.N. Antibacterial effect of sand blasted, large-grit, acid-etched treated Ti–Ag alloys. *Mater. Res. Bull.* **2012**, *47*, 2952–2955. [[CrossRef](#)]



© 2019 by the authors. Licensee MDPI, Basel, Switzerland. This article is an open access article distributed under the terms and conditions of the Creative Commons Attribution (CC BY) license (<http://creativecommons.org/licenses/by/4.0/>).